JOURNAL OF SOLID STATE CHEMISTRY **140,** 417–427 (1998)
ARTICLE NO. SC987910

Structural, Infrared, and Magnetic Characterization of the Solid Solution Series $Sr_{2-x}Pb_x(VO)(VO_4)_2$; Evidence of the Pb^{2+} $6s^2$ Lone Pair Stereochemical Effect

Olivier Mentre,* Anne-Claire Dhaussy,* Francis Abraham,* and Hugo Steinfink†,[1]

*Laboratoire de Cristallochimie et Physicochimie du Solide, URA CNRS 452, ENSCL, Universite des Sciences et Technologies de Lille, BP 108, 59652 Villeneuve, d'Ascq Cedex, France; and †Texas Materials Institute and Department of Chemical Engineering University of Texas at Austin, Austin, Texas 78712-1063

Received February 19, 1998; revised May 18, 1998; accepted May 27, 1998

The solid solution $Sr_{2-x}Pb_xV_3O_9$, $0 \le x \le 2$, was prepared by solid state reactions and characterized by X-ray diffraction, IR spectroscopy, and magnetic susceptibility measurements. Single crystals of the pure strontium phase and mixed Sr/Pb compounds were prepared by high temperature treatment of the respective powder compositions. $Pb_2V_3O_9$ crystals could only be obtained by the electrochemical reduction of molten PbV_2O_6. These crystals were always twinned. The previously reported crystal structure of $Sr_2V_3O_9$ was confirmed. It was refined to $R = 0.050$, $R_w = 0.057$, in space group C2/c, $a = 7.555(1)$ Å, $b = 16.275(2)$ Å, $c = 6.948(1)$ Å, $\beta = 119.78(1)^\circ$. The single crystal structural studies of the $Sr_{1.02}Pb_{0.98}V_3O_9$ and $Sr_{0.67}Pb_{1.33}V_3O_9$ members of the series show that the introduction of lead gives rise to a progressively complicated splitting of Sr^{2+}/Pb^{2+} and the tetrahedral vanadium ion crystallographic sites. As a consequence the vanadium framework distorts and beyond the $Sr_{0.5}Pb_{1.5}V_3O_9$ composition the crystal symmetry becomes triclinic. This distortion is ascribed to the stereochemical effect of the $6s^2$ lone pair of Pb^{2+}. The crystallographic parameters of $Pb_2V_3O_9$ are $a = 7.598(1)$ Å, $b = 16.393(3)$ Å, $c = 6.972(2)$ Å, $\alpha = 91.38(1)^\circ$, $\beta = 119.35(1)^\circ$, $\gamma = 90.47(1)^\circ$. $Pb_2V_3O_9$ exhibits a more complex IR spectrum than the monoclinic phases. Despite the similarity between the triclinic and monoclinic phases the magnetic susceptibilities indicate differences in the coupling between V^{4+} ions at low temperatures. © 1998 Academic Press

INTRODUCTION

The research reported here continues previous studies on mixed valence vanadium compounds containing di- and trivalent M cations ($M = Pb^{2+}$, Ba^{2+}, Bi^{3+}) (1–3). These phases display complex structural, electric, and magnetic properties due to the ability of vanadium to adopt several oxidation states and oxygen environments. Similarly, the vanadium bronzes $A_xV_2O_5$ ($A = Li^+$, Na^+, K^+, Mg^{2+}, Cu^{2+}, Ag^+) are also of current interest (4–6). Further impetus for the study of vanadium-containing compounds has been provided by the success of hydrothermal synthesis methods, leading to numerous new strontium and barium phospho-vanadates (7–10). During our attempts to prepare lead vanadium oxides by electrochemical reduction methods we always isolated twinned crystals of $Pb_2V_3O_9$. The phase diagram study of $MO - V_2O_5$ (M = Ca, Sr, Ba) by Bouloux *et al.* (11) revealed the existence of $Sr_2V_3O_9$ whose structure has been published (12). It is not isostructural with, but is closely related to, the structure of $Pb_2V_3O_9$, as shown by their powder diffraction patterns. The crystal structure and physical properties of $Ba_2V_3O_9$ have recently been published (2, 13). Although it has a common stoichiometry with the strontium and lead phases it is not isostructural, but nevertheless it exhibits similarities in the structural and magnetic features. This paper deals with the synthesis, crystal structure, infrared, and magnetic properties of the solid solution series $Sr_{2-x}Pb_xV_3O_9$, $0 \le x \le 2$, and in particular it evaluates the effect of the lone-pair $6s^2$ electrons of Pb^{2+} on the structure.

EXPERIMENTAL

Synthesis

Crystals of $Pb_2V_3O_9$ were grown by electrochemical reduction of PbV_2O_6 fused at 650°C in an alumina crucible contained in a steel vessel. The electrolysis was performed for 6 h under flowing nitrogen. Nickel wire was used as the electrodes. The potential applied to the electrodes was set to 3 V, yielding an initial current of 200 mA that progressively increased to 500 mA after 6 h. The anode was attacked during the experiment, leading to a small diffusion of Ni in the melt which could explain the current change. Black parallepiped crystals were mechanically isolated from the

[1] Author to whom correspondence should be addressed.

0022-4596/98 $25.00

melt. Pure $Pb_2V_3O_9$ powder was obtained by heating a mixture of $Pb_2V_2O_7$ and VO_2 in a 1:1 molar ratio at 600°C in an evacuated silica tube for 5 days. $Pb_2V_2O_7$ was previously prepared by heating a mixture of PbO and V_2O_5 in a 2:1 molar ratio at 700°C for 3 days. VO_2 was prepared by the reaction of V_2O_5 and V_2O_3 at 800°C under vacuum. V_2O_3 was synthesized by reducing V_2O_5 in a H_2 flux at 850°C.

$Sr_2V_3O_9$ was synthesized according to Bouloux *et al.* (11). $Sr_2V_2O_7$ was first prepared by the reaction at 700°C between $SrCO_3$ and V_2O_5 for 3 days. The product was then added to VO_2 in a 1:1 molar ratio and heated in an evacuated silica tube at 900°C for 5 days. Single crystals were obtained from the mixture of starting materials heated at 1020°C for 4 days in a sealed vycor tube, cooled at 4°C/h to 850°C and then furnace cooled. The preparation contains red single crystals of $Sr_2V_3O_9$ from which a crystal for the crystal structure determination was selected.

The solid solutions $Sr_{2-x}Pb_xV_3O_9$ were prepared by the reaction between $Sr_2V_2O_7$, $Pb_2V_2O_7$, and VO_2 for $x = 0.5$, 1, and 1.5 in a 700°C–900°C temperature range, depending on the Sr/Pb ratio. The mixture was first placed in a gold tube, which was introduced into a vycor tube that was then sealed under vacuum. Intermediate grinding was necessary to produce single phase materials. The heating of the powder products at 1000°C followed by cooling at 5°C/h yielded single crystals of the mixed Sr-Pb oxides. Indeed, a second heating of $SrPbV_3O_9$ powder gave rise to $Sr_{1.02}Pb_{0.98}V_3O_9$ single crystals while $Sr_{0.65}Pb_{1.35}V_3O_9$ single crystals were isolated from the inhomogeneous, reheated $Sr_{0.5}Pb_{1.5}V_3O_9$ mixture. X-ray diffraction powder patterns were obtained with a D 5000 Siemens apparatus. Values of the unit cell parameters were obtained by least-squares refinement of indexed powder patterns.

Infrared and Magnetic Measurements

Infrared data for $Sr_2V_3O_9$ and $Pb_2V_3O_9$ were collected on a fast Fourier transform Perkin-Elmer 1730 spectrometer in the 1500–400 cm^{-1} region. The samples were pelleted in a KBr matrix and the air spectrum was corrected from the obtained data. Magnetic susceptibilities were measured with a Quantum Design DC SQUID magnetometer over the interval 6–300 K for zero-field-cooled (ZFC) samples and over the range 300–6 K for field-cooled (FC) samples. The measurements for ZFC were taken by equilibrating the sample at 6 K, switching on a magnetic field of 1 kOe, and recording the magnetization as a function of the temperature to 300 K. With the applied field on, measurements of the susceptibility were then continued while the sample was cooled from 300 to 6 K to obtain FC data. Conductivity measurements performed with a conventional four-probe cell showed insulating behavior for both $Sr_2V_3O_9$ and $Pb_2V_3O_9$.

Single Crystal X-Ray Analysis

The $Sr_2V_3O_9$ crystal structure has been described in space group I2/a (12). It was transformed to C2/c in order to facilitate its comparison to the Pb^{2+}-substituted compounds studied here. Weissenberg photographs confirmed the 2/m Laue symmetry and observed extinctions were consistent with Cc and C2/c space groups first predicted by Bouloux *et al.* (11). The diffraction data were collected with a Philips PW 1100 for $Sr_2V_3O_9$ and $Sr_{0.67}Pb_{1.33}V_3O_9$. An Enraf Nonius CAD-4 automated diffractometer was used for the $Sr_{1.02}Pb_{0.98}V_3O_9$ data collection. Conditions for the data collections are given in Table 1. The intensities were corrected for Lorentz and polarization effects. Absorption corrections were applied using the analytical method of De Meulenaer and Tompa (14) with μ corresponding to the predicted stoichiometry at first and then improved with the exact value calculated from the refined stoichiometry. The crystal structure was successfully solved and refined in C2/c. The atomic scattering factors for neutral atoms were taken from "International Tables for X-Ray Crystallography" (15) and values for the anomalous dispersion correction from Cromer and Liberman (16). The full matrix least-squares refinement was performed with a local modification of the SFLS-5 program (17). The Patterson function located the strontium atoms in two independent 4(e) sites $(0,y,\frac{1}{4})$. Vanadium and oxygen atoms were subsequently located from Fourier electron density difference syntheses.

The crystal structure of $Sr_2V_3O_9$ (12) was redone so that the parameters determined with the local instrumentation and software will be comparable with the parameters of the solid solution series. The refinement of the atomic coordinates, anisotropic cation displacement parameters, and isotropic for oxygen, a secondary extinction parameter, and the introduction of a weighting scheme yielded $R = 0.050$ and $R_w = 0.057$ for 2480 reflections with $I > 3\sigma(I)$. The parameters in space group C2/c are shown in Table 2.

The refinement of $Sr_{1.02}Pb_{0.98}V_3O_9$ converged to $R = 0.037$ and $R_w = 0.036$. The cationic distributions Pb/Sr = 0.540(5)/0.460 and 0.484(5)/0.516 were obtained for the two 4(e) mixed occupancy sites. For the structure determination of $Sr_{0.67}Pb_{1.33}V_3O_9$ the Sr/Pb ratio 0.25/0.75 was initially assigned to both 4(e) cationic sites. This arbitrary distribution corresponds to the stoichiometry of the starting mixture from which single crystals were extracted. Least-squares refinement yielded 0.36(1)/0.64 for Sr(1)/Pb(1) and 0.31(1)/0.69 for Sr(2)/Pb(2), a much lower Pb^{2+} ratio than expected. The Fourier electron density difference syntheses exhibited strong maxima on both sides of the Sr/Pb sites but anisotropic displacement parameters did not remove them. These atoms were consequently split in half, occupying 8(f) positions. Anisotropic displacement parameters for the cations, refinement of occupancies, and introduction of a weighting scheme yielded $R = 0.068$ and $R_w = 0.057$. An

TABLE 1
Data, Intensity Measurement, and Structure Refinement Parameters for $Sr_{2-x}Pb_xV_3O_9$

	$Sr_2V_3O_9$	$Sr_{1.02}Pb_{0.98}V_3O_9$	$Sr_{0.67}Pb_{1.33}V_3O_9$
Crystal Data			
Crystal Symmetry	Monoclinic	Monoclinic	Monoclinic
Space Group	C2/c	C2/c	C2/c
Cell Dimension (Å)	a = 7.555(1)	a = 7.574(2),	a = 7.588(1)
	b = 16.275(2)	b = 16.321(5),	b = 16.35(2)
	c = 6.948(1)	c = 6.956(2),	c = 6.958(8)
	$\beta = 119.78(1)^\circ$	$\beta = 119.65(1)^\circ$	$\beta = 119.64(5)^\circ$
Volume ($Å^3$)	741.49	747.28	750.51
Density (calc., $g.cm^{-3}$)	4.20	5.260	5.61
Z	4	4	4
Data Collection			
Equipment	Philips PW 1100	CAD-4 Enraf-Nonius	Philis PW 1100
λ (MoKα (graphite monochromator)	0.7107 Å	0.7107 Å	0.7107 Å
Scan mode	ω–2θ	ω–2θ	ω–2θ
Scan Width (°)	1.2	$1.6 + 0.34 \tan\theta$	1.1
θ range (°)	2–36	2–35	2–36
Standard Reflections measured every 2 hours (no decay)	$00\bar{2}$, $\bar{2}2\bar{1}$, $20\bar{2}$	$13\bar{2}$, $\bar{1}51$, $\bar{1}50$, $20\bar{2}$, $02\bar{2}$	$\bar{2}00$, $00\bar{2}$, $20\bar{2}$
Recording Reciprocal Space	$-12 \le h \le 12$,	$12 \le h \le 12$,	$12 \le h \le 12$,
	$-26 \le k \le 26$,	$-26 \le k \le 26$,	$-26 \le k \le 26$.
	$0 \le l \le 11$	$0 \le l \le 11$	$0 \le l \le 11$
Number of measured reflections	3647	2859	3653
Number of Reflections $I > 3\sigma(I)$	2480	2421	1267
Number of independent reflections	1254	1212	698
$\mu(cm^{-1})$ (for $\lambda K\alpha = 0.7107$ Å)	188.97	336.54	379.44
Limiting faces and distances (mm) from arbitrary origin	101 0.200	101 0.100	101 0.200
	$\bar{1}0\bar{1}$	$\bar{1}0\bar{1}$	$\bar{1}0\bar{1}$
	$10\bar{1}$ 0.030	$10\bar{1}$ 0.020	$10\bar{1}$ 0.008
	$\bar{1}01$	$\bar{1}01$	$\bar{1}01$
	010 0.040	010 0.035	010 0.010
	$0\bar{1}0$	$0\bar{1}0$	$0\bar{1}0$
	$\bar{1}11$ 0.030	$\bar{1}\bar{1}1$ 0.030	$\bar{1}11$ 0.005
	$\bar{1}\bar{1}1$ 0.040	$11\bar{1}$	
	$11\bar{1}$	$\bar{1}11$ 0.021	
Transmission factor range	0.21–0.36	0.12–0.30	0.26–0.53
Merging R factor	0.048	0.032	0.072
Refinement			
Number of refined parameters	72	71	75
$R = \sum\|\|Fo\| - \|Fc\|\|/\sum\|Fo\|$	0.050	0.037	0.060
$Rw = [\sum w(\|Fo\| - \|Fc\|)^2/\sum wFo^2]^{1/2}$	0.057	0.036	0.050
With $w = 1/\sigma(Fo)$			

attempt to distinguish Pb^{2+} from Sr^{2+} in their common sites by shifting only the Pb^{2+} from their previous 4(e) positions to 8(f) did not succeed, increasing drastically the strontium displacement parameters. Fourier electron density difference maps continued to show two strong maxima at both sides of V(1) and V(2). Partial delocalization of V(1) and V(2) from 4e to 8f sites yielded final values $R = 0.060$, $R_w = 0.050$. Refinement of occupancies were unsuccessful but the best results were obtained for fixed V(1)′/V(1) and V(2)′/V(2) of 30% with a fixed value of their isotropic displacement parameters, 0.40 $Å^2$. The atomic coordinates and the anisotropic displacements parameters for the three compounds are shown in Tables 2 and 3. The program LAZY-PULVERIX (18) was used to obtain the observed and calculated X-ray powder patterns for $Sr_2V_3O_9$ and $Pb_2V_3O_9$, Table 4. The calculated intensities for $Sr_2V_3O_9$ are based on the single-crystal structure results.

Crystals of $Pb_2V_3O_9$ prepared electrochemically were always twinned. Weissenberg and precession photographs of the twin indicated a triclinic, pseudo-monoclinic, symmetry with systematic absences, hkl: $h + k + l = 2n + 1$, consistent with an I-centered Bravais lattice. The parameters of the triclinic unit cell are $a_I \approx 7.21$ Å, $b_I \approx 16.46$ Å, $c_I \approx 6.93$ Å, $\alpha_I \approx 91^\circ$, $\beta_I \approx 116^\circ$, and $\gamma_I \approx 90^\circ$. After

TABLE 2
Atomic Positions Occupancies, Positional Parameters, and Equivalent Isotropic Displacement Parameters, Å²

Atom		Site	Occ.	x	y	z	Beq (Å²)
Sr(1)/Pb(1)	*a*	4e	1	0	− 0.12735(4)	1/4	1.07(2)
	b	4e	0.540(5)/0.46	0	− 0.12554(3)	1/4	1.62(2)
	c	8f(1/2)	0.36(1)/0.64	0.0079(39)	− 0.1249(1)	0.2361(41)	1.67(21)
Sr(2)/Pb(2)		4e	1	0	0.4516(4)	1/4	0.96(2)
		4e	0.484(5)/0.52	0	0.45223(3)	1/4	1.74(2)
		8f(1/2)	0.31(1)/0.69	− 0.0247(18)	0.4525(1)	0.2369(39)	1.59(25)
V(I)		4e	1	0	0.65981(7)	1/4	0.57(3)
		4e	1	0	0.6602(1)	1/4	0.63(4)
		4e	0.70(n.r.)	0	0.6589(8)	1/4	0.53(12)
V(1)′		—	—		—	—	—
		—	—	—	—	—	—
		8f(1/2)	0.30(n.r)	0.0361(29)	0.6633(22)	0.2890(30)	0.40(n.r)
V(2)		4e	1	0	0.07930(7)	1/4	0.62(3)
		4e	1	0	0.07986(8)	1/4	0.73(4)
		4e	0.70(n.r.)	0	0.0793(11)	1/4	0.73(14)
V(2)′		—	—	—	—	—	—
		—	—	—	—	—	—
		8f(1/2)	0.30(n.r.)	0.0290(36)	0.0826(27)	0.2844(35)	0.40(n.r.)
V(3)		8f	1/2	0.28453(3)	0.75531(2)	0.0339(3)	0.59(6)
		8f	1/2	0.2897(3)	0.7553(1)	0.0399(3)	0.52(7)
		8f	1/2	0.2961(8)	0.7558(4)	0.0478(10)	1.55(20)
O(1)		8f	1	0.1691(6)	0.7241(2)	0.2250(7)	1.01(10)
		8f	1	0.1669(7)	0.7234(3)	0.2221(8)	1.33(13)
		8f	1	0.1637(19)	0.7225(7)	0.2187(21)	1.93(45)
O(2)		8f	1	0.1630(6)	0.0200(3)	0.2197(8)	1.37(11)
		8f	1	0.1622(7)	0.0202(3)	0.2198(8)	1.46(14)
		8f	1	0.1632(20)	0.0207(7)	0.2212(24)	2.46(51)
O(3)		8f	1	0.3864(6)	0.0977(2)	0.0247(6)	1.02(10)
		8f	1	0.3857(7)	0.0974(3)	0.0253(8)	1.30(13)
		8f	1	0.3888(20)	0.0971(7)	0.0248(21)	1.90(45)
O(4)		8f	1	0.8573(6)	0.1393(2)	0.0096(6)	0.96(10)
		8f	1	0.8581(7)	0.1394(3)	0.0113(8)	1.11(12)
		8f	1	0.8552(18)	0.1397(6)	0.0092(21)	1.32(38)
O(5)		4e	1	0	0.2871(3)	1/4	0.90(13)
		4e	1	0	0.2869(3)	1/4	0.99(17)
		4e	1	0	0.2837(6)	1/4	1.65(33)

$a = Sr_2V_3O_0$, $b = Sr_{1.02}Pb_{0.98}V_3O_9$, $c = Sr_{0.67}Pb_{1.33}V_3O_9$; the n.r. notation is used for not refined parameters.

transforming to a C-centered cell the parameters are $a_C \approx 7.49$ Å, $b_C \approx 16.46$ Å, $c_C \approx 6.93$ Å, $\alpha_C \approx 91^\circ$, $\beta_C \approx 120^\circ$, and $\gamma_C \approx 90^\circ$. This unit cell is very close to that of $Sr_2V_3O_9$ and indicates their isotypic character. Also, long exposure photographs of $Pb_2V_3O_9$ crystals show weak $h0l$: $l = 2n + 1$ reflections violating c-glide symmetry. It is evident that $Pb_2V_3O_9$ is nearly isostructural with $Sr_2V_3O_9$ but the introduction of the $6s^2$ lone-pair causes slight distortions of the crystal structure. The unit cell parameters, $a = 7.598(1)$ Å, $b = 16.393(3)$ Å, $c = 6.972(2)$ Å, $\alpha = 91.38(1)^\circ$, $\beta = 119.35(1)^\circ$, $\gamma = 90.47(1)^\circ$ were obtained from a least squares refinement of the powder diffraction pattern.

The twin operation is caused by a mirror perpendicular to the *b* axis. The $0kl$ Weissenberg photographs of a twinned crystal showed that a mirror plane perpendicular to b^* separated $00l$ and $00\bar{l}$ reflections by 2°. Thus in the $0kl$ octant reflections of $0kl$ and $0k\bar{l}$ were adjacent. In the $1kl$ Weissenberg the separation between adjacent $1kl$ and $1k\bar{l}$ reflections increased. Rietveld refinement of a powder X-ray diffraction pattern based on the parameters of $Sr_{0.67}$

TABLE 3
Anisotropic Displacement Parameters $\exp[-(\beta_{11}h^2 + \beta_{22}k^2 + \beta_{33}l^2 + 2\beta_{12}hk + 2\beta_{13}hl + 2\beta_{23}kl)]$

		β_{11}	β_{22}	β_{33}	β_{12}	β_{13}	β_{23}
Pb(1)/Sr(1)	a	0.0053(1)	0.00083(2)	0.0098(2)	0	0.0038(1)	0
	b	0.0116(1)	0.00126(2)	0.01555(2)	0	0.0084(1)	0
	c	0.013(1)	0.00116(6)	0.022(2)	0.0003(2)	0.0174(8)	0.00015(28)
Pb(2)/Sr(2)		0.0065(1)	0.00061(2)	0.0081(2)	0	0.0041(1)	0
		0.0143(1)	0.00101(1)	0.0132(1)	0	0.0095(1)	0
		0.009(2)	0.00133(6)	0.0712(2)	0.0001(2)	0.011(2)	− 0.00001(29)
V(1)		0.0031(2)	0.00045(3)	0.0036(2)	0	0.0009(2)	0
		0.0042(3)	0.00051(4)	0.0050(3)	0	0.0032(4)	0
		0.002(1)	0.0005(1)	0.0027(9)	0	0.002(5)	0
V(2)		0.0061(4)	0.0060(5)	0.0075(5)	0	0.006(4)	0
		0.0038(3)	0.00049(4)	0.0065(4)	0	0.0028(3)	0
		0.0005(11)	0.0007(2)	0.006(1)	0	0.008(4)	0
V3		0.0030(5)	0.00043(5)	0.0042(6)	0.00003(14)	0.0008(4)	− 0.00007(15)
		0.0019(6)	0.00044(6)	0.0043(7)	0.0003(1)	0.0014(5)	0.0002(1)
		0.002(2)	0.0003(2)	0.007(2)	0.0002(5)	0.004(1)	0.00002(64)

$a = Sr_2V_3O_9$, $b = Sr_{1.02}Pb_{0.98}V_3O_9$, $c = Sr_{0.67}Pb_{1.33}V_3O_9$.

$Pb_{1.33}V_3O_9$ was not satisfactory. It appears that the complete substitution of the $6s^2$ ion, Pb^{2+}, distorts the structure sufficiently that refinement did not converge. A complete structure determination will be published separately.

DISCUSSION

Structural Features

Selected bond distances and bond angles for $Sr_2V_3O_9$, $Sr_{1.02}Pb_{0.98}V_3O_9$ and $Sr_{0.65}Pb_{1.35}V_3O_9$ are given in Table 5. In these compounds the V(3) atom is displaced from the center of a VO_6 octahedron to an 8(f) site. This environment is consistent with a vanadyl V^{4+} ion. The electrostatic bond strengths add to 4.03 (19) for this site occupant in the pure strontium material. V(1) and V(2) atoms are located at the centers of VO_4 tetrahedra. The calculated valence sums are 5.15 and 5.12, respectively, in agreement with the expected V^{5+} ion occupying such a site.

The previously determined crystal structure of $Sr_2V_3O_9$ (12) is described here in space group C2/c, in conformity with the structures of the solid solution series. It is formed by infinite chains of $V(3)^{4+}O_6$ octahedra sharing O(5) corners (Figs. 1, 2). The chains run parallel to the $\mathbf{a} + \mathbf{c}$ diagonal at $y = \frac{1}{4}$ and $\frac{3}{4}$. The octahedra are tilted and the distances between adjacent O(4) atoms of neighboring octahedra are 2.942(7) and 3.926(8) Å, respectively. The V(2) tetrahedra bridge adjacent octahedra by sharing the closer O(4) atoms on alternate sides of the chain. The chains are bridged laterally by V(1) tetrahedra sharing O(1) atoms forming a two-dimensional plane. The planes are held together by Sr^{2+} ions that balance the negative charge on the layers.

The short V(3)–O(3), 1.657(2) Å is characteristic of vanadyl (IV) compounds and is about 0.35 Å shorter than the four equatorial V–O bonds. The sixth oxygen is weakly bonded trans to the V=O bond. A V^{4+} octahedral coordination is commonly found in vanadium oxides, although several exceptions have been reported. For instance, Sr_2VO_4 exhibits isolated tetrahedral V^{4+} (20) while MV_3O_7 (M = Cd, Ca, Sr) have layer structures that include two kinds of edge sharing VO_5^{6-} square pyramids with apical V=O bonds ranging from 1.57 to 1.64 Å (21a, 21b). Nevertheless, some octahedral V^{3+}/V^{4+}-containing oxides do not show the presence of V=O bonds because of delocalization

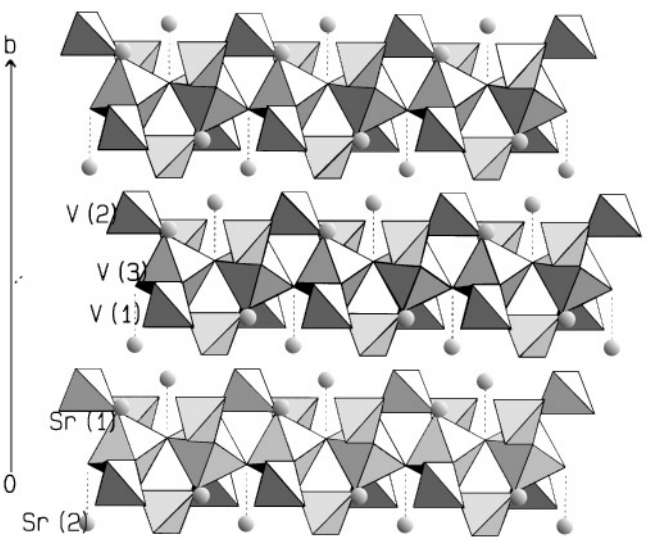

FIG. 1. Projection of the $Sr_2V_3O_9$ crystal structure on the $(10\bar{1})$ plane emphasizing the infinite chains.

TABLE 4
X-Ray Powder Patterns for $Sr_2V_3O_9$ and $Pb_2V_3O_9$ Compounds ($\lambda = 1.54056$ Å)

hkl		$Sr_2V_3O_9$				$Pb_2V_3O_9$		
$Sr_2V_3O_9$	$Pb_2V_3O_9$	2θobs.	2θcalc.	Iobs./Io	Icalc./Io	2θobs.	2θcalc.	Iobs./Io
020	020	n.o.	10.86	n.o.	1.3	10.79	10.79	40.3
021	02$\bar{1}$	n.o.	18.30	n.o.	3.7	17.88	17.88	30.9
	021					18.45	18.45	43.5
130	1$\bar{3}$0	21.25	21.24	3.5	4.7	20.82	20.83	18.8
	130					21.31	21.31	24.3
040	040	21.82	21.83	7.4	4.5	21.68	21.68	36.1
111	1$\bar{1}$1	25.12	25.11	25.2	32.9	24.68	24.68	13.0
	111					25.02	25.02	20.3
22$\bar{1}$	2$\bar{2}\bar{1}$	n.o.	26.01	n.o.	0.0	n.o.	25.81	7.3
	22$\bar{1}$					25.94	25.94	n.o.
041	04$\bar{1}$	26.40	26.40	4.5	6.9	25.81	25.82	28.2
	041					26.62	26.62	11.0
200	200	27.17	27.18	41	46.1	26.92	26.91	60.9
20$\bar{2}$	20$\bar{2}$	28.55	28.56	100	88.6	28.50	28.50	100
220	2$\bar{2}$0	29.35	29.35	19.7	21	28.84	28.83	12.2
	220					29.29	29.31	5.1
002	002	29.60	29.60	42.6	49.8	29.39	29.38	60.4
131	1$\bar{3}$1	n.o.	29.58	n.o.	24.2	n.o.	28.85	7.9
	131					29.74	29.75	n.o.
150	1$\bar{5}$0	30.65	30.64	19.8	19.7	30.13	30.12	17.3
	150					30.69	30.70	23.6
	22$\bar{2}$	n.o.	30.64	n.o.	0.1	30.25	30.43	9.3
	2$\bar{2}\bar{2}$					n.o.	30.67	n.o.
15$\bar{1}$	15$\bar{1}$	30.95	30.95	98.4	100	30.63	30.62	58.2
	1$\bar{5}\bar{1}$					30.92	30.92	60.5
022	02$\bar{2}$	31.61	31.62	8.1	14.3	n.o.	31.04	n.o.
	022					n.o.	31.72	n.o.
24$\bar{1}$	24$\bar{1}$	n.o.	32.34	n.o.	2.1	32.03	32.04	4.4
	24$\bar{1}$					32.26	32.25	5.6
060	060	33.01	33.00	6.4	3.4	32.77	32.77	9.1
240	2$\bar{4}$0	35.12	35.12	25	30.2	34.41	34.41	9.1
	240					35.22	35.22	6.8
24$\bar{2}$	24$\bar{2}$	36.23	36.23	10.3	10.7	n.o.	35.88	8.0
	2$\bar{4}\bar{2}$					36.29	36.29	n.o.
31$\bar{1}$	3$\bar{1}\bar{1}$	36.49	36.49	3.3	3.5	n.o.	36.16	n.o.
	31$\bar{1}$					n.o.	36.31	n.o.
151	1$\bar{5}$1	37.07	37.07	31	41.3	36.13	36.13	22.0
	151					37.35	37.35	26.8
15$\bar{2}$	15$\bar{2}$	37.86	37.86	14.3	17.6	37.16	37.17	13.2
	1$\bar{5}\bar{2}$					n.o.	38.14	n.o

of the d^2/d^1 electrons over several crystallographic sites leading to semi-conductor or metallic behavior. The well known metallic $SrVO_3$ perovskite illustrates this feature (22). More complex oxides like $Ba_8V_7^{+3/+4/+5}O_{22}$, a semiconductor, also exhibits perfectly symmetric $V^{4+}O_6$ octahedra with six V–O distances of 1.942(1) Å (23). In α and β $MV_2(P_2O_7)_2$ (M = Sr, Ba), regular $V^{+4}O_6$ octahedra are connected to each other via phosphate tetrahedra, inhibiting any kind of itinerant electronic mobility (8, 24). In $Sr_2V_3O_9$, the vanadyl bond length is significantly longer than in compounds such as β-$Ba_2VO(PO_4)_2 \cdot H_2O$, 1.580(4) Å (7), or in $A(VO)_2(AsO_4)_2$ (A = Ba, Sr) 1.590(6) Å (10), but somewhat shorter than in $Ba_2V_3O_9$ 1.686(3) Å (2) whose structure consists of infinite, isolated rutile-like chains of edge sharing octahedra. The short V=O bond exists between the vanadium atoms and one of the bridging oxygen atoms. Thus, octahedral vanadium atoms are displaced cooperatively intrachain to avoid the formation of unlikely V=O=V entities. The same kind of cooperative V^{4+} shifting within the octahedra of the chains are expected in $Sr_2V_3O_9$ and, indeed, alternating short and long V–O distances of 1.657(2) Å, and 2.185(2) Å are observed. The Sr–O bond lengths range from 2.5 to 2.8 Å and bond valence sums are 1.89 and 1.91.

TABLE 5
Interatomic Distances (Å) and Selected Bond Angles (°) for the Crystals Studied

	$Sr_2V_3O_9$	$Sr_{1.02}Pb_{0.98}V_3O_9$	$Sr_{0.67}Pb_{1.33}V_3O_9$
Sr(1)/Pb(1) *Environment*			
Sr(1)/Pb(1)–O(1)^{i}	2.780(4)	2.821(5)	2.81(2)
Sr(1)/Pb(1)–O(1)^{iii}	2.780(4)	2.821(5)	2.88(2)
Sr(1)/Pb(1)–O(2)^{i}	2.735(4)	2.73(1)	2.71(2)
Sr(1)/Pb(1)–O(2)^{iii}	2.735(4)	2.73(1)	2.77(2)
Sr(1)/Pb(1)–O(3)^{ii}	2.620(4)	2.622(4)	2.63(3)
Sr(1)/Pb(1)–O(3)^{iv}	2.620(4)	2.622(4)	2.66(3)
Sr(1)/Pb(1)–O(4)^{ii}	2.527(5)	2.538(7)	2.45(4)
Sr(1)/Pb(1)–O(4)^{iv}	2.527(5)	2.538(7)	2.64(4)
⟨Sr(1)/Pb(1)⟩	2.665	2.677	2.693
Sr(2)/Pb(2) *Environment*			
Sr(2)/Pb(2)–O(2)^{v}	2.685(5)	2.699(8)	2.57(2)
Sr(2)/Pb(2)–O(2)^{vii}	2.685(5)	2.699(8)	2.84(2)
Sr(2)/Pb(2)–O(3)^{v}	2.740(9)	2.732(5)	2.69(2)
Sr(2)/Pb(2)–O(3)^{vi}	2.579(6)	2.591(6)	2.63(3)
Sr(2)/Pb(2)–O(3)^{vii}	2.740(9)	2.732(5)	2.78(2)
Sr(2)/Pb(2)–O(3)^{viii}	2.579(6)	2.591(6)	2.53(3)
Sr(2)/Pb(2)–O(4)^{vi}	2.809(4)	2.832(4)	2.69(1)
Sr(2)/Pb(2)–O(4)^{viii}	2.809(4)	2.832(4)	2.96(2)
Sr(2)/Pb(2)–O(5)	2.677(5)	2.699(5)	2.766(2)
⟨Sr(2)/Pb(2)⟩	2.72	2.712	2.717
V(1) *tetrahedron*			
V(1)–O(1)	1.725(5)	1.715(6)	1.72(2)
V(1)–O(1)^{iii}	1.725(5)	1.715(6)	1.72(2)
V(1)–O(3)^{v}	1.695(7)	1.704(5)	1.70(1)
V(1)–O(3)^{vii}	1.695(7)	1.704(5)	1.70(1)
⟨V(1)–O⟩	1.71	1.709	1.71
O(1)–V(1)–O()^{iii}	105.3(6)	106.1(8)	105(2)
2 × O(1)–V(1)–O(3)^{v}	109.2(6)	109.0(5)	108(1)
2 × O(1)–V(1)–O(3)^{vii}	113.2(7)	113.5(6)	115(2)
O(3)^{v}–V(1)–(3)^{vii}	106.8(6)	106.0(6)	107(2)
average	109.5	109.5	109.7
V(2) *tetrahedron*			
V(2)–O(2)	1.665(2)	1.661(9)	1.66(2)
V(2)–O(2)^{iii}	1.665(5)	1.661(9)	1.66(2)
V(2)–O(4)	1.765(3)	1.758(5)	1.78(2)
V(2)–O(4)^{iii}	1.765(3)	1.758(5)	1.78(2)
⟨V(2)–O⟩	1.715	1.709	1.72
O(2)–V(2)–O(2)^{iii}	107.8(7)	108(1)	109(2)
2 × O(2)–V(2)–O(4)	110.6(4)	110.4(8)	111(2)
2 × O(2)–V(2)–O(4)^{iii}	107.5(5)	107.5(8)	107(2)
O(4)–V(2)–O(4)^{iii}	112.8(5)	112.9(6)	113(2)
average	109.67	109.7	110
V(3) *octahedron*			
V(3)–O(1)	1.983(6)	1.977(7)	1.98(2)
V(3)–O(1)^{vi}	2.025(6)	2.035(7)	2.05(2)
V(3)–O(4)^{ii}	1.965(4)	1.985(5)	1.99(1)
V(3)–O(4)^{v}	1.997(4)	1.997(5)	1.99(1)
V(3)–O(5)^{ii}	2.185(2)	2.231(2)	2.270(5)
V(3)–O(5)^{v}	1.657(2)	1.623(2)	1.558(5)
⟨V(3)–O⟩	1.969	1.975	1.973

TABLE 5—*Continued*

V(3) *octahedron*			
O(1)–V(3)–O(4)^{ii}	86.5(3)	86.6(4)	86.7(9)
O(1)–V(3)–O(4)^{v}	92.6(4)	92.4(5)	92(1)
O(1)–V(3)–O(5)^{ii}	87.8(2)	86.2(3)	84.5(7)
O(1)–V(3)–O(5)^{v}	92.0(3)	94.0(4)	96(1)
O(1)^{vi}–V(3)–O(4)^{ii}	92.3(4)	91.1(4)	90(1)
O(1)^{vi}–V(3)–O(4)^{v}	84.5(3)	84.7(4)	84.2(9)
O(1)^{vi}–V(3)–O(5)^{ii}	77.1(2)	76.5(3)	75.3(6)
O(1)^{vi}–V(3)–O(5)^{v}	103.1(4)	103.3(4)	104(1)
O(4)^{ii}–V(3)–O(5)^{ii}	85.4(2)	83.8(3)	81.3(5)
O(4)^{ii}–V(3)–O(5)^{v}	94.7(3)	95.8(3)	98.4(8)
O(4)^{v}–V(3)–O(5)^{ii}	79.3(2)	78.7(2)	78.1(5)
O(4)^{v}–V(3)–O(5)^{v}	100.6(3)	101.7(4)	102.2(8)
average	89.66	89.57	82.72
V–V *lengths*			
V(3)–V(1)	3.535(3)	3.540(3)	3.56(1)
V(3)–V(1)^{vi}	3.416(3)	3.418(3)	3.44(1)
V(3)–V(2)^{ii}	3.398(2)	3.426(2)	3.47(2)
V(3)–V(2)^{v}	3.268(2)	3.250(2)	3.25(2)
V(3)–V(3)^{viii}	3.651(1)	3.666(1)	3.671(1)

Symmetry codes: ii = $\bar{x}$, $\bar{y}$, $\bar{z}$; iii = $\bar{x}$, y, 1/2 − z; iv = x, $\bar{y}$, 1/2 + z; v = 1/2 + x, 1/2 + y, z; vi = 1/2 − x, 1/2 − y, $\bar{z}$; vii = 1/2 − x, 1/2 + y, 1/2 − z; viii = 1/2 + x, 1/2 − y, 1/2 + z.

Pb^{2+} Substitution for Sr^{2+}

As shown in Fig. 3, the *a*, *b*, and *c* parameters increase with *x* while β decreases. At $x = 1.5$, the triclinic distortion appears but then remains almost unchanged from $x = 1.5$ to $x = 2$. The distortion is clearly visible on the X-ray powder pattern (Fig. 4). The very weak line at about 19.2° 2θ for the $x = 1.5$ composition is most likely due to an impurity.

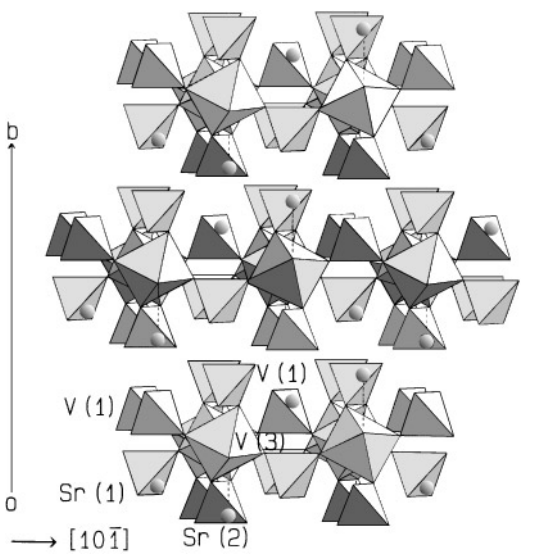

FIG. 2. Projection of the $Sr_2V_3O_9$ crystal structure on the (101) plane showing the interchain linkages.

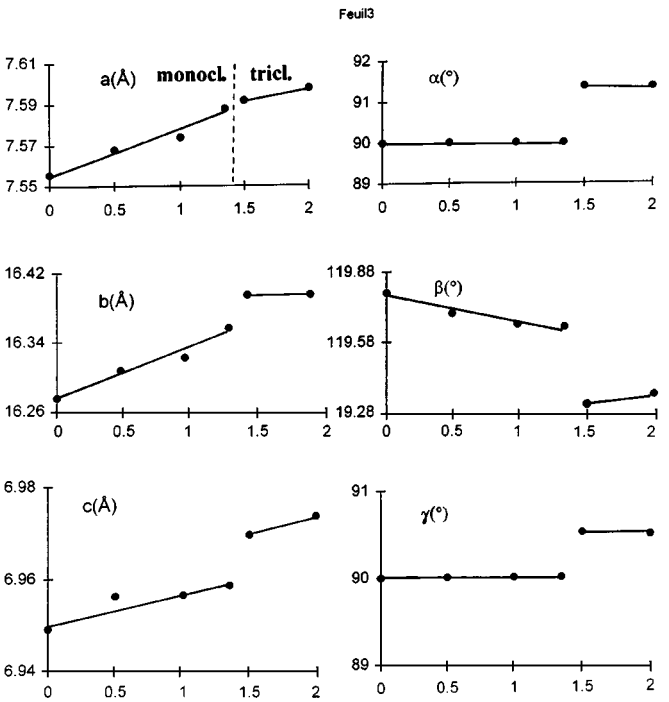

FIG. 3. Unit cell parameters vs x for $Sr_{2-x}Pb_xV_3O_9$ solid solutions.

The structural studies indicate that until at least the $Sr_{1.02}Pb_{0.98}V_3O_9$ composition, Pb^{2+} cations merely substitute for Sr^{2+} without any drastic structural change. As shown in Table 2, there are no significant changes in the Pb/Sr nor vanadium oxygen polyhedra. Nevertheless, one observes a significant increase of the isotropic displacement parameters for Pb/Sr(1) and Pb/Sr(2), 1.62(2) $Å^2$, and 1.74(2) $Å^2$, respectively, as compared to Sr(1), 1.07(2) $Å^2$ and Sr(2), 0.96(2) $Å^2$. The vanadium displacement parameters remain almost unchanged. The ionic radii Sr^{2+} 1.26 Å (VIII coord.), 1.31 Å (IX coord.)) are comparable to Pb^{2+} 1.29 Å (VIII coord.), 1.35 Å (IX coord.).

The Pb^{2+} or Bi^{3+} lone-pair effect on stereochemistry has been studied by several authors and is known to shift Pb^{2+} cations from a high symmetry position to a lower one (25–27). Recently the effect of the $6s^2$ lone-pair was shown to reduce the space group symmetry from $P6_3/mmc$ in NaV_6O_{11} to the noncentrosymmetric $P6_3mc$ in PbV_6O_{11} (1). It is also the main reason for the existence of incommensurate modulated structures as in α-PbO (28). The large values of the displacement parameters in the Pb substituted phases strongly suggest that the $6s^2$ lone-pairs are disordered around the central 4(e) site, Table 2. In $Sr_{0.67}Pb_{1.33}V_3O_9$ Pb^{2+} ions are the major site occupants and they are statistically distributed on both sides of the two fold axis. The main effect is the partial split of the tetrahedral vanadium atoms and the consequent high displacement parameters of the four tetrahedral oxygen atoms O(1)–O(4), 1.9(5), 2.5(5), 1.9(4) and 1.3(4) $Å^2$ as opposed to 1.01(10), 1.37(11), 1.02(10), and 0.96(10) for the same oxygen ions in $Sr_2V_3O_9$. These large values are most likely representative of the average position resulting from the superposition of three slightly shifted oxygen tetrahedra corresponding to three possible sites of the polyhedra V(1) + 2 V(1′) and V(2) + 2 V(2′). The splitting of the Sr^{2+}/Pb^{2+} cationic sites and of the tetrahedral vanadium with increasing Pb^{2+} substitution, while retaining the monoclinic structure, provide clues to the eventual transformation to the triclinic structure of $Pb_2V_3O_9$.

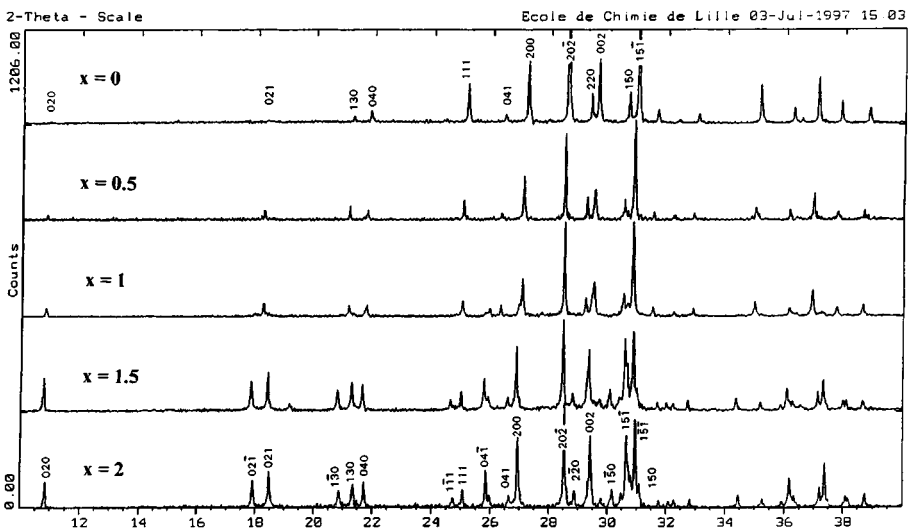

FIG. 4. X-ray powder pattern for the $Sr_{2-x}Pb_xV_3O_9$ solid solution series.

Infrared Data

The infrared spectra of the $x = 0$, 0.5, 1, 1.5, and 2 phases are shown in Fig. 5. They indicate a progressive change from $Sr_2V_3O_9$ to $Pb_2V_3O_9$. Only VO_4 and V=O vibrational modes are observed in the recorded region. Baran recently studied the vibrational spectroscopic characterization of $Sr_2V_3O_9$ in relation to its structural peculiarities (29). After a factor group analysis of the internal vibration of VO_4^{3-} and from the correlation of Raman and infrared data, he proposed the assignment given in Table 6. V=O is assigned to the 831 cm^{-1} medium intense band in the infrared spectrum and is characterized by its intense line in the Raman spectrum. On the basis of these results, the vibrational infrared spectra of the solid solution compounds were assigned as shown in Table 6. The complementary Raman spectrum for $Pb_2V_3O_9$ shows the most intense peak at 844 cm^{-1}. Thus the V=O vibration progressively shifts from 837 cm^{-1} for the strontium compound to 844 cm^{-1} in the lead compound. In the latter, the vanadyl band is included in the broad $\nu 3$ component appearing at 850 cm^{-1}. Two major features become evident when examining the complete spectra. A progressive disappearance of the strong 902 cm^{-1} $\nu 3$ component for the strontium phases and the growth of a weak 882 cm^{-1} band for $Pb_2V_3O_9$ and the simultaneous increase in the intensity of $\nu 1$ with Pb^{2+} substitution. Moreover, the different $\nu 4$ massifs observable in the low wavenumber region, including $\nu 3$ and $\nu 4$ bands, split into many complex weak bands for $Pb_2V_3O_9$, as compared to those of the $Sr_2V_3O_9$ spectrum. Such an observation is in good agreement with the lower local symmetry of vanadium atoms in a triclinic system, which lifts the degeneracy of the vibrational modes.

TABLE 6
Assignment of the Infrared Spectra of $Sr_{2-x}Pb_xV_3O_9$ Compounds (cm^{-1})

$x = 0$	$x = 0.5$	$x = 1$	$x = 1.5$	$x = 2$	Assignment
914 sh	—	—	—	—	$\nu_3(VO_4^{3-})$
902 vs	899 vs	894 s	885 w	882 w	
858 s	857 s	856 m	849 s	850 vs	$\nu_1(VO_4^{3-})$
837 w	835 w	834 w	840 sh	—	ν(V=O)
824 w	—	821 w	817 vw	819 w	
798 vs	793 vs	791 s	781 vs	783 vs	$\nu_3(VO_4^{3-})$
770 s	766 s	766 m	744 w	744 w	
719 vs	717 vs	712 vs	686 w	687 vw	
465 vs	461 vs	461 vs	459 m	461 m	$\nu_4(VO_4^{3-})$
—	—	—	434 m	430 m	

Note. s = strong; m = medium; w = weak; v = very; sh = shoulder.

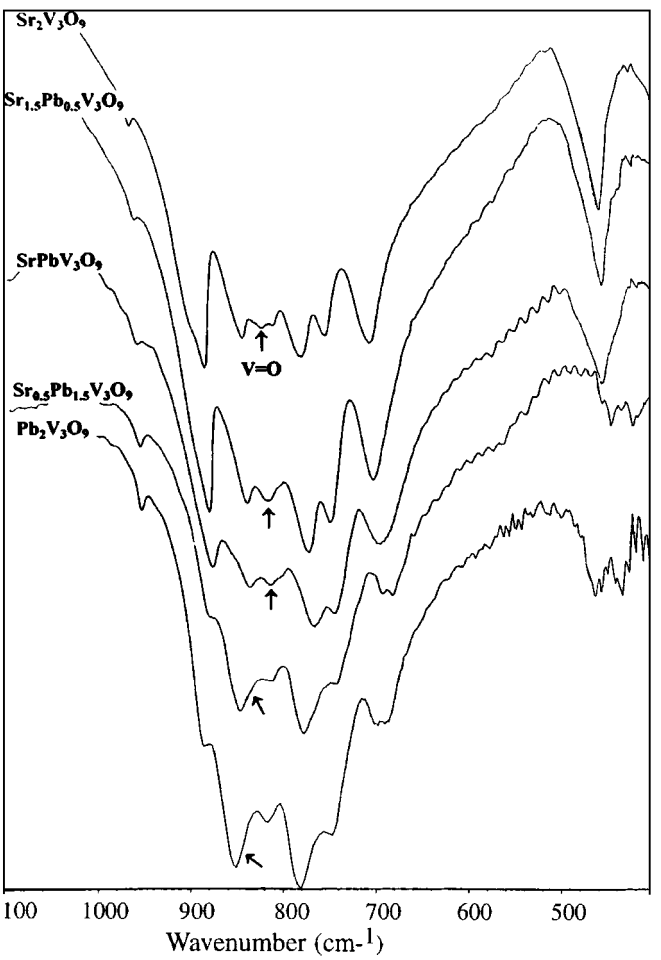

FIG. 5. Infrared spectra for (a) $Sr_2V_3O_9$ and (b) $Pb_2V_3O_9$.

The $\nu 1$ and $\nu 3$ bands show a systematic shift towards lower wavenumbers from strontium to the lead phases. Thus, for $Sr_2V_3O_9$ the four $\nu 3$ strong components appear at 719, 770, 798, and 902 cm^{-1}, respectively, while in $Pb_2V_3O_9$ they occur at 687–699, 744, 783, and 882 cm^{-1}. The $\nu 1$ and $\nu 3$ frequencies are respectively the symmetric and the asymmetric V–O stretching vibrations and are bond-length dependent. Although the V–O tetrahedral bond distances remain unchanged at least until $x = 1.33$, Table 5, this effect is probably due to the $6s^2$ Pb^{2+} ion presence.

Magnetic Properties

Susceptibility data for $Sr_2V_3O_9$ and $Pb_2V_3O_9$ showed the onset of antiferromagnetic ordering at $T_N = 50$ and 25 K, respectively, and paramagnetic behavior above these temperatures, Figs 6a and b. The paramagnetic data were modeled using $\chi^{-1} = (T - \theta)/C$, where χ is the measured susceptibility, C is the Curie constant, T is the temperature (K), and θ is the Curie–Weiss constant. A least squares fit yielded $\theta = -105.6$ K and -21.2 K, respectively. The

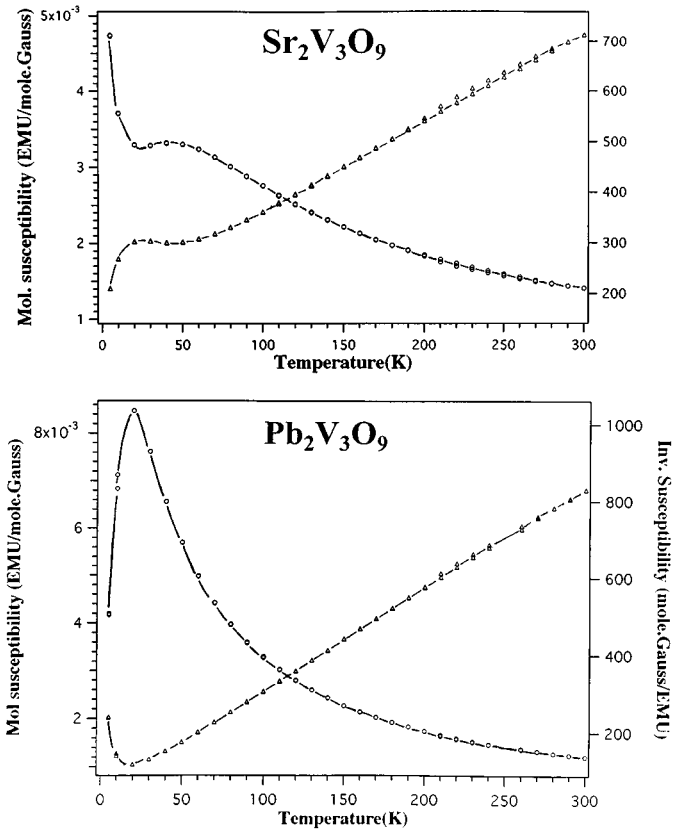

FIG. 6. Temperature dependencies of magnetic susceptibility (circles) and its inverse (triangles) of a polycrystalline specimen of (a) $Sr_2V_3O_9$ and (b) $Pb_2V_3O_9$.

calculated value $\mu_{eff} = 2.1\ \mu_B$ per formula unit for $Sr_2V_3O_9$ is slightly higher than the expected value of $1.73\ \mu_B$ for a V^{4+} spin only consideration. This is probably due to incomplete quenching of the orbital contribution for this cation. For $Pb_2V_3O_9$ $\mu_{eff} = 1.73\ \mu_B$. The increase of χ below about 21 K for $Sr_2V_3O_9$ is most likely due to the presence of a small amount of paramagnetic impurity. A similar behavior was also observed in $Ba_2V_3O_9$ (2). There, arguments were advanced based on its crystal structure that it could also be due to a parasitic ferromagnetic component of a canted-spin antiferromagnetic ordering (2). A similar argument can be made for $Sr_2V_3O_9$.

The susceptibility of $Pb_2V_3O_9$ differs from that of a typical antiferromagnet in which the decrease in susceptibility as the temperature approaches zero should not be less than one-half of the maximum value reached close to the Neel point. In fact the general shape of the susceptibility curve resembles that of the classic $s = \frac{1}{2}$ dimer Heisenberg model first proposed by Bleaney and Bowers (30). The magnetic structure at low temperatures could be interpreted as V^{4+} ions associated in binary clusters, rather than in a linear chain. This hypothesis is reinforced by the $1.73\ \mu_B$ value of the effective moment. This value fits the theory and is also observed for VO_2 whose structure changes to vanadium pairs below 340 K (31). It is often observed in octahedral chain frameworks as in $Cu(NO_3)_2 \cdot 2.5H_2O$ (32) or Sr_3ZnIrO_6 (33). In $Pb_2V_3O_9$ such a transition might be induced by the Pb^{2+} disorder that prevents a linear V–V arrangement.

ACKNOWLEDGMENTS

The authors thank Nicole Muhlenbein for the IR spectroscopy. O. Mentre and H. Steinfink thank the Welch Foundation, Houston, Texas for financial support.

REFERENCES

1. O. Mentre and F. Abraham, *J. Solid State Chem.* **125,** 91 (1996).
2. A. C. Dhaussy, F. Abraham, O. Mentre, and H. Steinfink, *J. Solid State Chem.* **126,** 328 (1996).
3. F. Abraham and O. Mentre, *J. Solid State Chem.* **109,** 127 (1994).
4. J. M. Savariault, J. L. Parize, D. Ballivet-Tkatchenko, and J. Galy, *J. Solid State Chem.* **122,** 1 (1996).
5. P. Rozier, J. M. Savariault, and J. Galy, *J. Solid State Chem.* **122,** 303 (1996).
6. V. Shklover, T. Haibach, F. Ried, R. Nesper, and P. Navak, *J. Solid State Chem.* **123**, 317 (1996).
7. W. T. A. Harrison, J. T. Vaughey, A. J. Jacobson, D. P. Goshorn, and J. W. Johnson, *J. Solid State Chem.* **116,** 77 (1995).
8. L. Benhamada, A. Grandin, M.M. Borel, A. Leclaire, and B. Raveau, *Acta Crystallogr. C* **47,** 2437 (1991).
9. K. H. Lii, T. C. Lee, S. N. Liu, and S. W. Wang, *J. Chem. Soc. Dalton Trans.* **1,** 1051 (1993).
10. S. L. Wang and C. Y. Cheng. *J. Solid State Chem.* **109,** 277 (1994).
11. J. C. Bouloux, J. Galy, and P. Hagenmüller, *Rev. Chim. Miner.* **11,** 48 (1974).
12. J. Feldmann and Hk. MüllerBuschbaum, *Z. Naturforsch. B* **50,** 43 (1995).
13. J. Feldmann and Hk. MüllerBuschbaum, *Z. Naturforsch. B* **51,** 489 (1995).
14. J. De Meulenaer and H. Tompa, *Acta Crystallogr.* **19,** 1014 (1965).
15. "International Tables for X-Ray Crystallography," Vol. IV. Kynoch Press, Birmingham, 1974.
16. D. T. Cromer and D. Liberman, *J. Chem. Phys.* **531,** 1891 (1970).
17. C. T. Prewitt, "SFLS-5, Report ORNL-TM 305," Oak Ridge National Laboratory,Oak Ridge, Tenessee, 1966.
18. K. Yvon, W. Jeitschko, and E. Parthe, *J. Appl. Cryst.* **10,** 73 (1977).
19. I. D. Brown and D. Altermatt, *Acta Crystallogr. B* **41,** 244 (1985).
20. W. Gong, J. E. Greedan, G. Liu, and M. Bjorguinsson, *J. Solid State Chem.* **94,** 213 (1991).
21a. J.-C. Bouloux and J. Galy, *Acta Cryst. B* **29,** 269 (1973).
21b. G. Liu and J. E. Greedan, *J. Solid State Chem.* **103,** 139 (1993).
22. V. Giannakopoulou, P. Odier, J. M. Bassat, and J. P. Loup, *Solid State Comm.* **93,** 579 (1995).
23. G. Liu and J. E. Greedan, *J. Solid State Chem.* **108**, 371 (1994).
24. S. J. Hwu, R. I. Carroll, and D. L. Serra, *J. Solid State Chem.* **110,** 290 (1994).
25. L. Nistor, G. Van Tendeloo, S. Amelinckx, V. Kahlenberg, and H. Böhm, *J. Solid State Chem.* **119,** 281 (1985).

26. P. B. Moore, P. K. Sen Gupta, and Y. Le Page, *Am. Mineralog.* **74,** 1186 (1989).
27. J. Galy and R. Enjalbert, *J. Solid State Chem.* **44,** 1 (1982).
28. D. Le Bellac, J. M. Kiat and P. Garnier, *J. Solid State Chem.* **114,** 459 (1995).
29. E. J. Baran, *J. Raman Spectrosc.* **27,** 555 (1996).
30. B. Bleaney and K. D. Bowers, *Proc. R. Soc. London A* **214,** 451 (1952).
31. J. B. Goodenough, "Magnetism and the Chemical Bond," Interscience, New York London, 1963.
32. L. Berger, S. A. Friedberg, and J. T. Schriempf, *Phys. Rev.* **132,** 1057 (1963).
33. T. N. Nguyen, Ph.D. thesis, Massachussets Institute of Technology, May 1994.